

Supplementary Information

Laser 3D printing of Complex Copper Structures

Loic Constantin,^{1,2,‡} Zhipeng Wu,^{1, ‡} Nan Li,¹ Lisha Fan,^{1,} Jean-Francois Silvain^{1,2,*} and,*

Yong Feng Lu,^{1,}*

¹ Department of Electrical and Computer Engineering, University of Nebraska-Lincoln, Lincoln, NE, 68588-0511, USA.

² CNRS, Univ. Bordeaux, Bordeaux INP, ICMCB, UMR 5026 F-33608 Pessac, France.

³ Département Générale de l'Armement - DGA/DS/Mission pour la Recherche et l'Innovation Scientifique, 92221 Bagneux, France.

1. Powder and part analysis (SEM and XRD)

Figure S1 presents the X-ray diffraction (XRD) diffractograms of the printed 3D part and Cu powders. Diffraction peaks at $2\theta = 36, 43, 50$ and 74° are observed and attributed to (-111) , (111) , (200) and (220) planes of the face-centered cubic Cu. No other peaks were identified, implying that Cu is the only crystalline phase before and after printing.

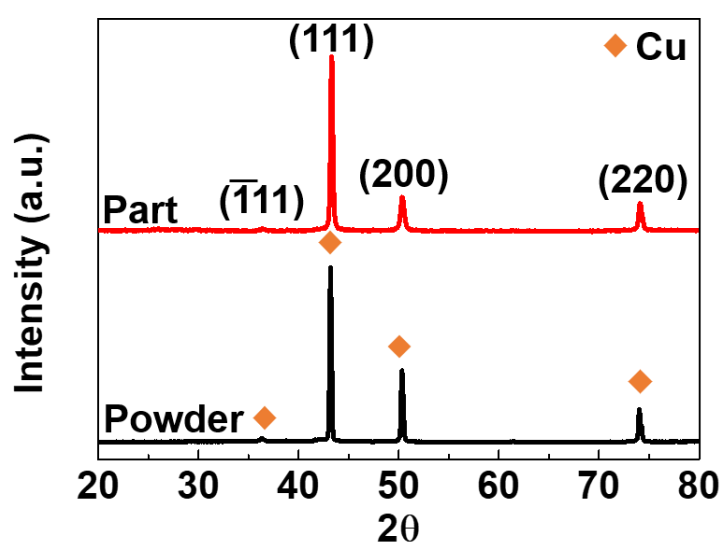


Figure S1. XRD diffractograms of the printed part, and Cu powders.

In addition to XRD diffractograms, energy dispersive X-Ray (EDX) was performed on the Cu powder and part. **Figure S2 (a)** and **(b)** show the SEM micrographs of the Cu powder and polished Cu part (printing parameters: power = 400 W, layer thickness = 0.03 mm, scan speed = 400 mm/s and hatch distance = 0.12 mm), respectively. **Figure S2 (c)** and **(d)** shows the EDX point spectra of the Cu powder and the part, respectively. **Figure S2 (e)** summarizes the EDX analyses where it can be observed that the powder presents about 7.7 wt.% of oxygen while the Cu part shows an oxygen content of 2.4 wt.%

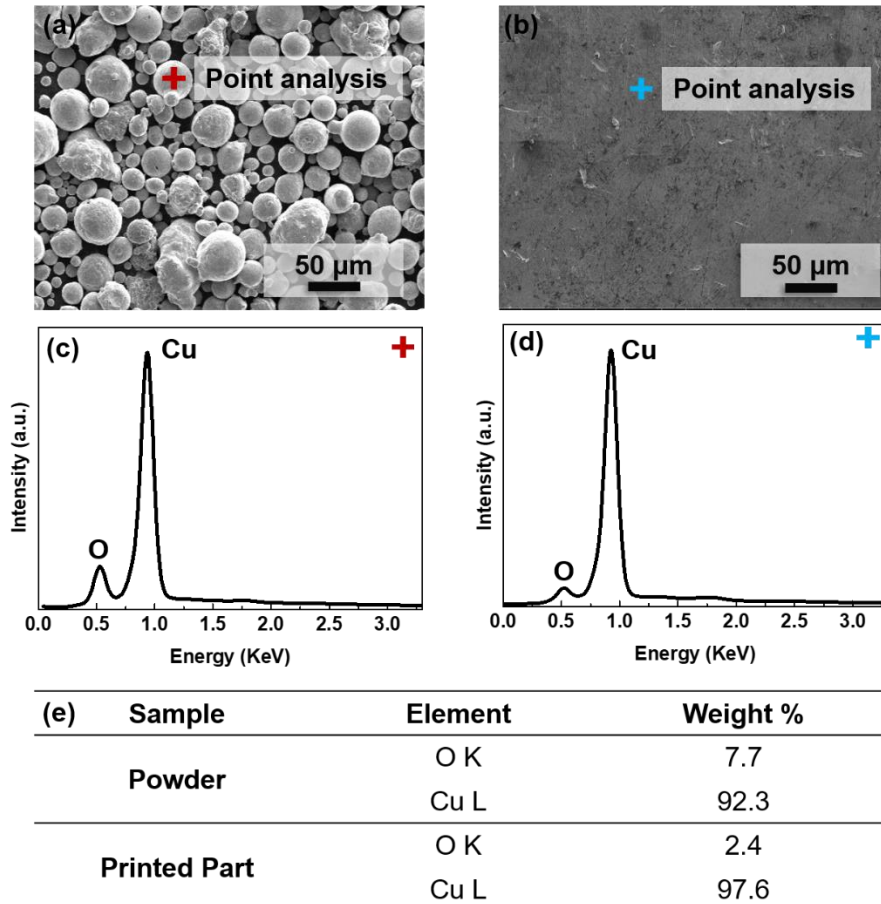


Figure S2. (a) and (b) SEM micrographs of Cu powder and part, (c) and (d) EDX point spectra and (e) summarized EDX analyses.

2. SLM 125 laser characteristics

The SLM 125 3D printer is equipped with a 400 W single-mode continuous wave (CW) fiber laser (IPG photonics, Yb: YAG, $\lambda = 1070$ nm). The laser beam has a stigmatic Gaussian profile, indicating a TEM₀₀ mode, as shown in **Figure S3 (a)**. **Figure S3 (b)** lists the parameters of the laser beam and are conform to the EN ISO 11146-2 measurement method. The beam is focused to 0.5 mm on the build plate (Z_0). The powder bed surface and beam were manually fine-tuned to the focal point by adjusting the vertical position of the build plate. The beam has a diameter of 63 μm at the focal point and a Rayleigh length of 2.5 mm. The quality of the laser beam is

evaluated by the beam quality factor (BPP) and the effective beam quality factor (M^2). It is measured that the BPP has a value of 0.396 mm/rad and an M^2 of 1.16. The results imply an excellent beam quality when focused to a small spot with the conservation of the original output power.

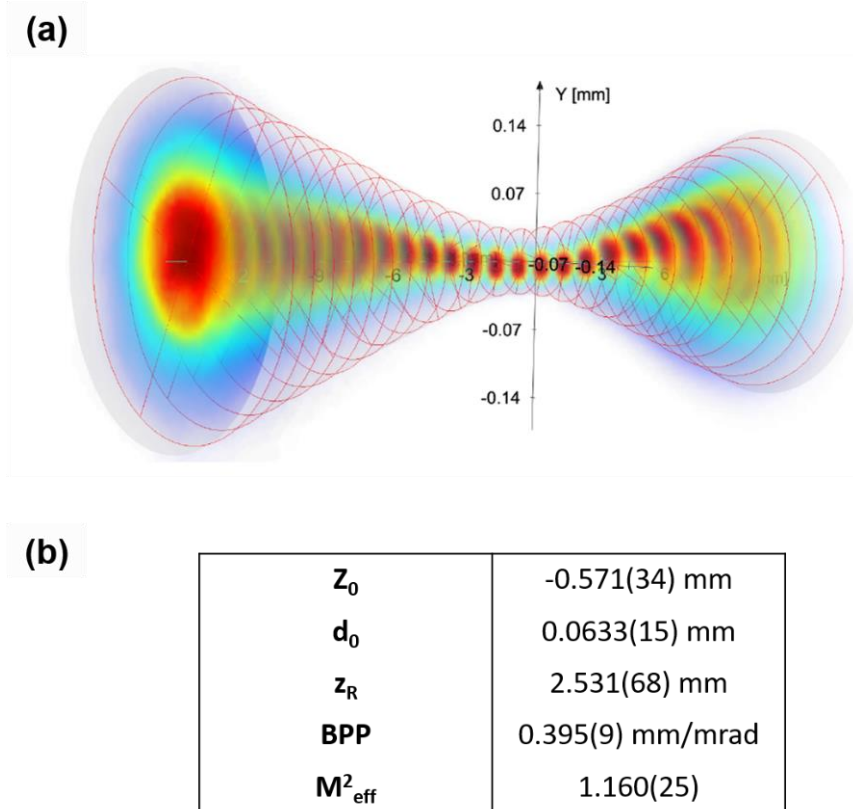


Figure S3. (a) Laser beam profile, and (b) beam characteristics.

3. Electrical conductivity measurements

Figure S4 (a) shows a schematic illustration of the sample preparation for the four-point probe and hardness measurements. The heat sink pillars were cut from the base plate for electrical conductivity measurement, while the base plate was used for hardness tests (see next section). The four-point probe method was carried out using a Keithley 2400 Source Meter (accuracy $\sim 1 \mu\Omega$) for a current range between -0.03 to 0.03 A. The length and diameter of the pillars were

measured using a digital caliper (accuracy 0.01 mm). **Figures S4 (b) and (c)** display the current/voltage (I/V) curve for the commercial (COM) and printed heat sinks, respectively. The resistance was calculated by linear regression of the I/V curve. As shown in **Figures S4 (b) and (c)**, the resistance of the printed and COM heat sinks is 144 and 155 $\mu\Omega$. The resistance was converted into electrical conductivity using the following equation:

$$\sigma = \frac{L}{A \times R}, \quad (1)$$

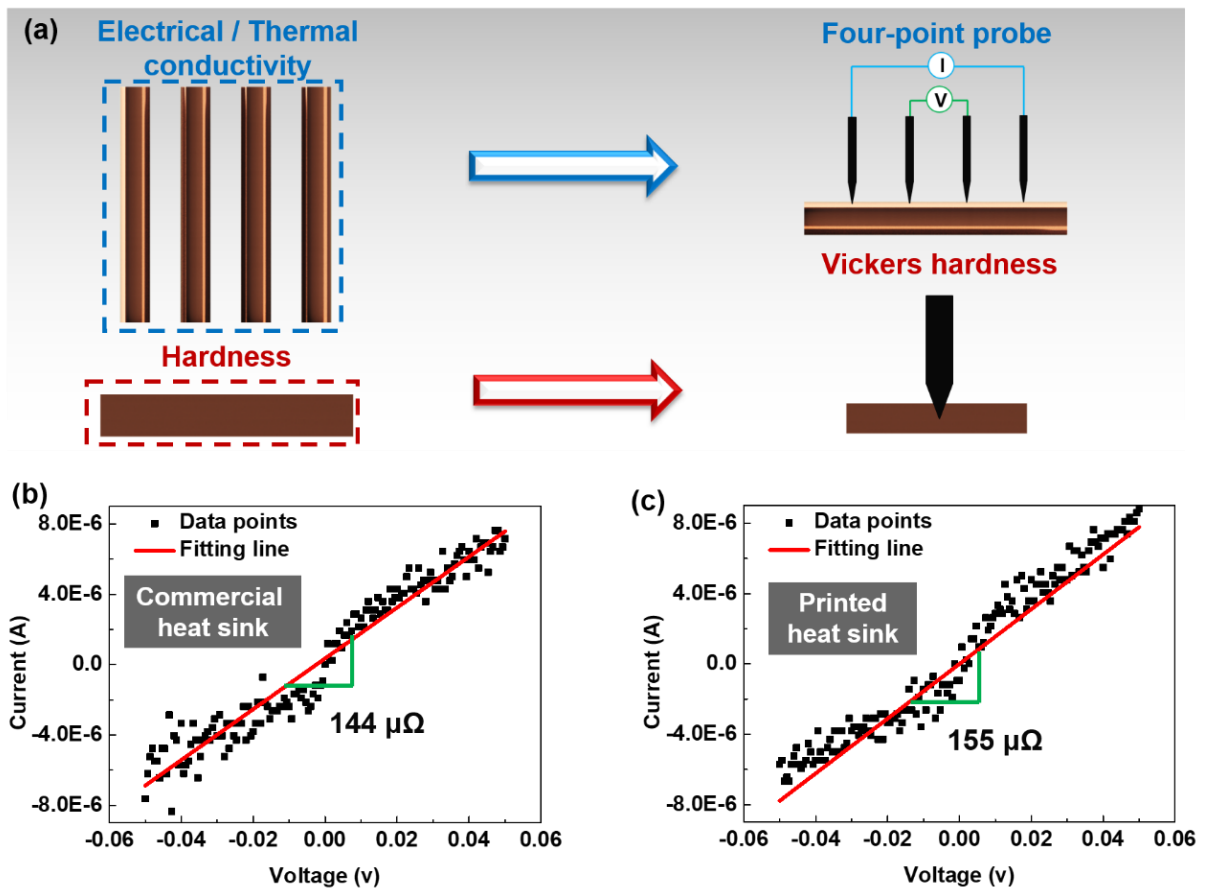


Figure S4. (a) Schematic illustration of the sample preparation for measurements of the physical properties; I/V curves of (b) commercial (COM) and (c) printed heat sinks.

where σ is the electrical conductivity (S/m), L is the length of the pillar (m), A is the area cross-section (m^2), and R the resistance (Ω). The computation leads to electrical conductivities for

the COM and printed heat sinks of 5.81×10^7 and 5.71×10^7 S/m, respectively. The electrical conductivities were then converted into the international annealed copper standard percentage (IACS%) with a value of 5.8×10^7 S/m for pure Cu. Finally, IACS% values for the COM and printed heat sinks are 100 and 98 IACS%, respectively.

4. Vickers Hardness tests

The heat-sink base plate was used for the Vickers hardness tests using a Wilson Tukon™ 2500-3 with a load and dwell time of 0.5 kg and 10 s, respectively. The hardness was calculated using the following equation:

$$HV \approx 1.891 \times \frac{F}{d^2}, \quad (2)$$

where F is the force of the indenter in N and d is the average length of the diagonal in mm.

Figure S5 (a) shows the SEM micrographs of the indentation of the printed and COM heat sink bases. It can be seen that the diagonals of the COM heat sink are more significant than the printed one. Ten indentations were performed and averaged to obtain an accurate value of the hardness. The grain size was measured to understand the difference in the hardness between the COM and printed heat sinks (COM = 72 MPa and Printed = 108 MPa). For that, the heat-sink bases were etched in a solution composed of 23% HNO₃ and 77% H₂O for a time of 10 s.

Figure S5 (b) shows the SEM micrographs the COM and printed heat sinks after acid etching. It can be observed that the grain sizes of the COM and printed heat sinks are about ~22 and ~30 μm .

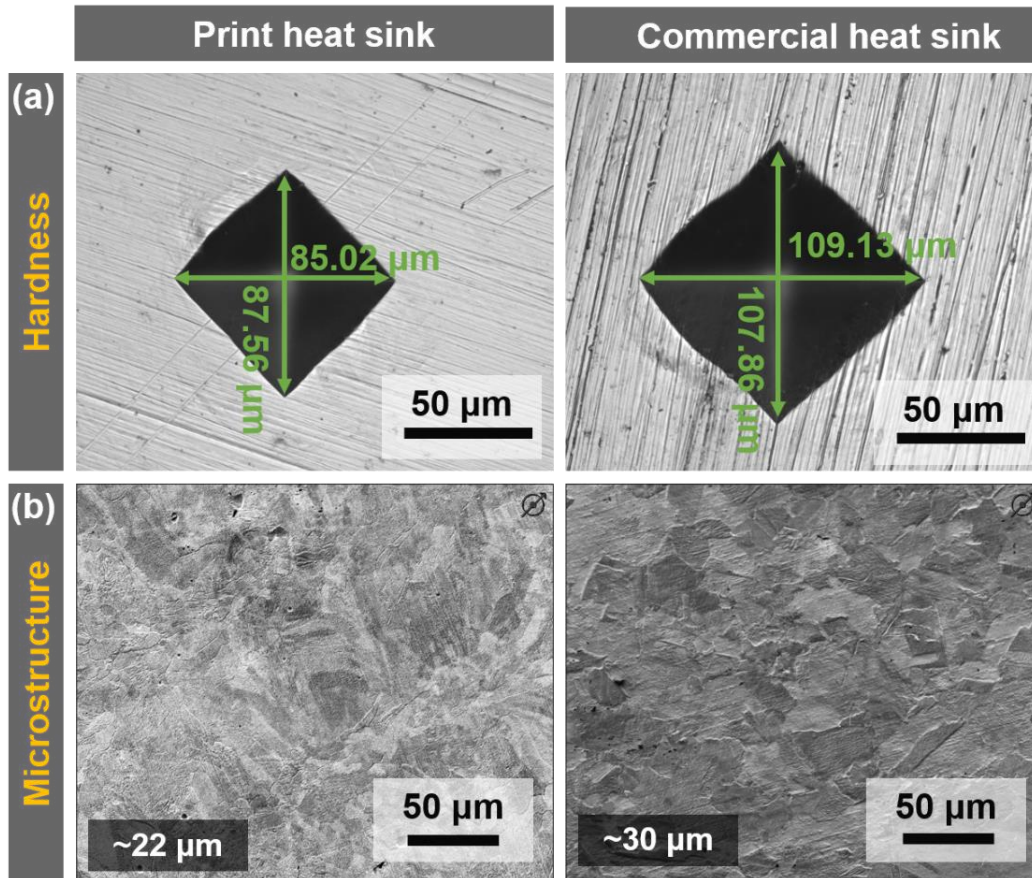


Figure S5. SEM micrographs of commercial (COM) and printed heat-sink base plates after (a) Vickers hardness tests and (b) acid etching

5. Heat-dissipation performance measurements

The thermal performance of the different heat sink structures was measured, as illustrated in **Figure 6 (a)** in the manuscript. **Figure S6** and **S7** show the infrared (IR) images of each structure after a chip being heated on a hot plate to 100, 150, and 200 °C for 5 min with the equivalent chip temperature vs. time plots. As can be seen in **Figure S6 (a)** and **S7 (a)**, at a heating temperature of 100 °C, the chip temperature reaches a value of about 83 °C. Also, the temperature of the chip with the COM, printed, helix, and tubes heat sink structures is similar (IR images) and measured to be 66, 66, 67, and 66 °C, respectively. However, when the hot

plate temperature rises to 150 °C, (**Figure S6 (b)** and **S7 (b)**) a difference starts to appear with a measured temperature of the chip with the COM, printed, helix and tubes heat sinks structures of 99, 99, 95, and 90 °C, respectively. The temperature of the chip without a heat sink is about 123 °C. At even higher temperatures (200 °C), a significant difference between each structure can be seen. The chip temperatures with the COM, printed, helix, and bent heat sink structures are measured to be 130, 130, 123, and 115 °C, respectively, in contrast to 166 °C for the chip alone (**Figure S6 (c)** and **S7 (c)**).

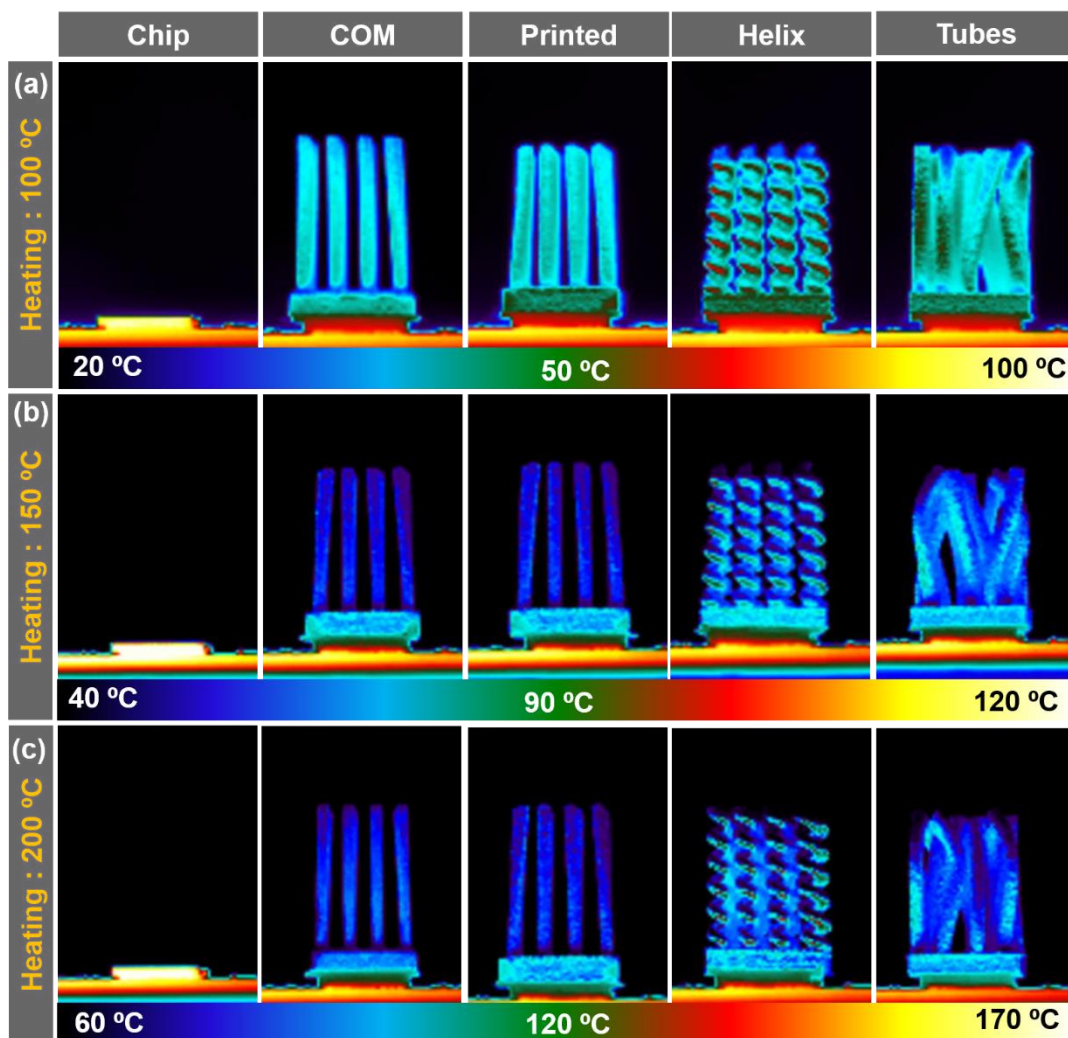


Figure S6. IR images of chip alone, and with COM, printed, helix, and tubes heat sinks heated at (a) 100, (b) 150, and (c) 200 °C, respectively.

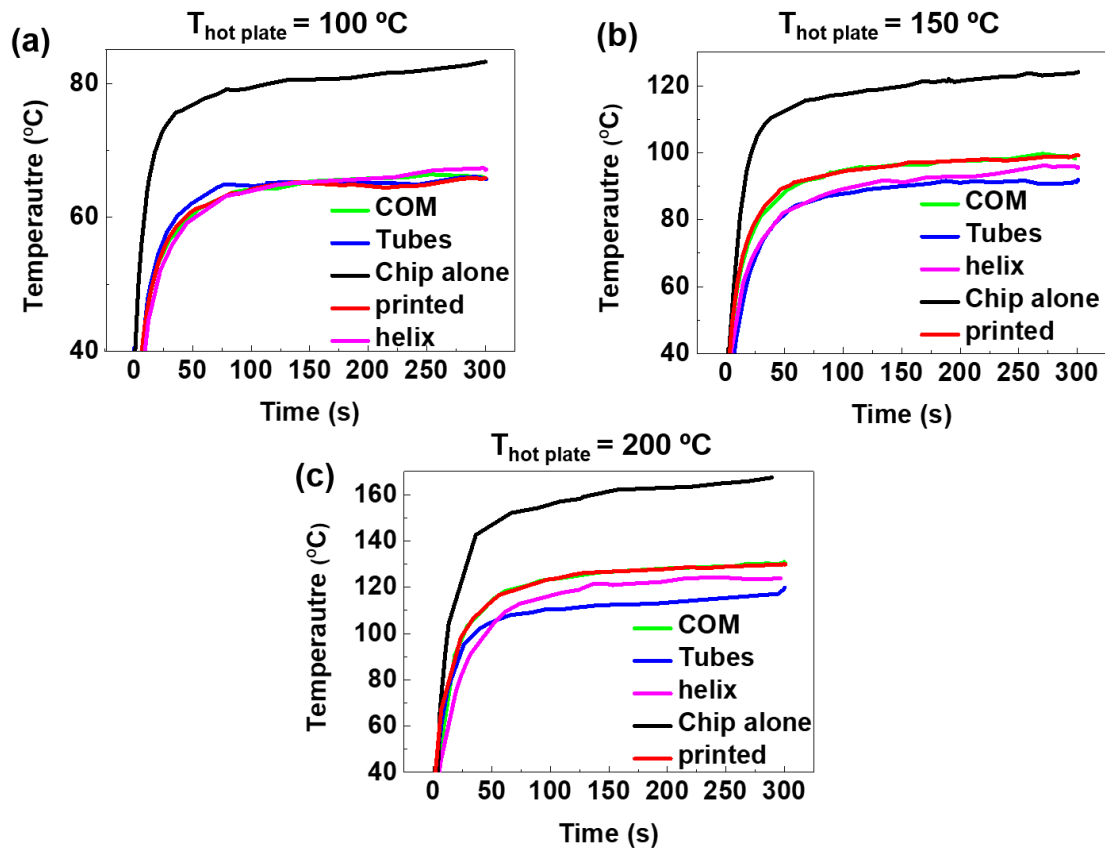


Figure S7. Chip temperature vs. time plots for different heat sinks structures heated at (a) 100, (b) 150, and (c) 200 °C, respectively.